J Mater Sci (2009) 44:949–953
DOI 10.1007/s10853-008-3182-0

Effect of pre-deformation on the precipitation process and magnetic properties of Fe–Cu model alloys

Yasuhiro Kamada · Seiki Takahashi · Hiroaki Kikuchi · Satoru Kobayashi · Katsuyuki Ara · Junichi Echigoya · Yusuke Tozawa · Kenta Watanabe

Received: 24 September 2008 / Accepted: 10 December 2008 / Published online: 13 January 2009

Abstract The effect of pre-deformation on the precipitation process and magnetic properties of Fe–Cu model alloys was investigated. These specimens simulate irradiation embrittlement of nuclear reactor pressure vessel (RPV) steels. Fe–1 wt%Cu alloys with and without pre-deformation in solid-state solution were thermally aged at 773 K for various times and the evolution of hardness, conductivity, and microstructure were investigated. Pre-deformation enhanced Cu precipitation and caused precipitation at dislocations. The coercive force tended to decrease for the pre-deformed specimen and the underlying mechanism is discussed. The results obtained are related to the magnetic characteristics of irradiated RPV steels.

Introduction

Aging degradation of nuclear power plant (NPP) components is of great concern for safe operation of aged NPPs. Irradiation embrittlement of reactor pressure vessels (RPV) in NPPs is one of the crucial aging problems and is caused by the formation of irradiation defects like Cu-rich precipitates [1–4]. Development of non-destructive evaluation (NDE) techniques for these precipitates is a key to solve the problem and the magnetic NDE method is a strong candidate because of its high sensitivity to the formation of lattice defects [5–7]. Since handling of neutron irradiated specimens is not easy due to their radioactivity, non-radioactive specimens are often used to simulate irradiated microstructures in feasibility studies. Thermally aged Fe–Cu model alloys containing Cu precipitates are typical specimens and magnetic properties of these alloys have been investigated by several groups [8–11]. However, all previous reports on Fe–Cu model alloys have focused on precipitation effects for simplicity and neglected the effects of other lattice defects. Actual RPV steels like A533B have a complex bainite microstructure with various kinds of lattice defects including dislocations. It is thus important to check the influence of these defects by further experiments. This study highlights the role of dislocations by adopting pre-deformed Fe–Cu model alloys. The effect of pre-deformation on the thermal precipitation process and magnetic properties was investigated and multiple effects due to coexistence of dislocations and precipitates are discussed.

Y. Kamada (✉) · S. Takahashi · H. Kikuchi · S. Kobayashi · K. Ara · J. Echigoya · Y. Tozawa · K. Watanabe
NDE & Science Research Center, Faculty of Engineering, Iwate University, Morioka 020-8551, Japan
e-mail: kamada@iwate-u.ac.jp

Experimental procedures

The chemical composition of the Fe–Cu model alloy is listed in Table 1. Plates of Fe–1 wt%Cu alloys were water-quenched from 1123 K to prepare a supersaturated solid-solution state. One of the quenched plates was cold-rolled successively. The former plate is designated undeformed and the latter plate is pre-deformed. Four shaped specimens were taken from both the undeformed plate and the pre-deformed plate by an electrical-discharged wire cutting machine and isothermally aged at 773 K by systematically varying the aging time. The following three experiments were carried out to determine differences in precipitation processes. Micro-Vickers hardness was conducted for block specimens under a load of 300 g at five points and averaged. Electrical conductivity was measured at room

Table 1 Chemical composition (wt%) of Fe–1 wt%Cu specimens

C	Si	Mn	P	S	Al	Cu	N	O
0.0010	<0.01	<0.01	0.001	0.0004	<0.001	1.03	0.0015	0.0085

temperature for thin rod specimens ($25 \times 0.5 \times 0.5$ mm^3) by a direct current four-point method. In addition to the isothermally aged Fe–1 wt%Cu specimens, the conductivities of as-quenched specimens with different Cu content from 0 to 1.2 wt% were also measured to clarify the Cu concentration dependence. Structural characterization was performed using a high-voltage transmission electron microscope (TEM) operated at an acceleration voltage of 1250 kV. Disk specimens for TEM were prepared by standard techniques such as mechanical polishing by fine sandpaper and electro-polishing in a twin-jet system using a solution of 10% perchloric and 90% acetic acid. Magnetic properties were also investigated, and magnetic hysteresis curves (B–H curves) were measured using a lab-made digital loop tracer for ring-shaped specimens. The outer and inner diameters of the specimens were 18 and 12 mm, respectively, and the height was 2 mm. The specimens were wound with excitation and detection coils consisting of 62 turns. Induced voltage signals collected by a pre-amplifier and a low-pass filter were digitized and integrated to evaluate the flux density, B. The excitation field value, H, calculated from a current signal was combined with the flux density to obtain B–H curves. The excitation field and frequency used were 3.8 kA/m and 0.05 Hz, respectively. The reduction ratio of cold-rolling was 10% except for TEM specimen which was 40%. In each measurement of the characteristics, the isothermal aging and measurement were executed cyclically for one specimen to avoid data scattering due to inherent variations of batch characteristics. The aging time represented here is thus an integrated time.

Results

Vickers hardness

Figure 1 shows the aging time dependence of Vickers hardness for pre-deformed and undeformed specimens. Both specimens were hardened by precipitation. In the undeformed specimen the hardness shows a peak which can be explained by considering structural changes of precipitates from coherent to incoherent and also coarsening (so-called overaging) [12, 13]. The hardness behavior of the pre-deformed specimen had two stages: the first was an abrupt increase by thermal aging and the second was a peak similar to the other specimen (arrows in Fig. 1). The

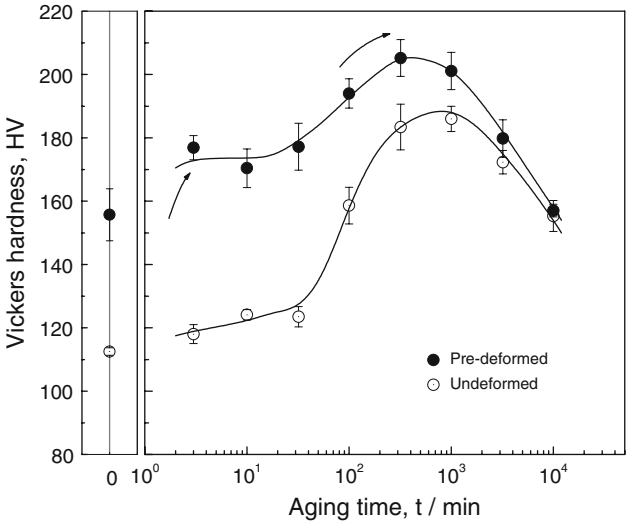

Fig. 1 Aging time dependence of the Vickers hardness for pre-deformed and undeformed Fe–Cu alloys

former trend is due to enhancement of precipitation caused by the high nucleation rate at dislocations [12, 13]. This phenomenon was also confirmed by other experiments as described below.

Electrical conductivity

Figure 2 shows the aging time dependence of conductivity for pre-deformed and undeformed Fe–Cu alloys together with the value for pure iron. Both conductivities increased with increasing aging time and reached at around the value of iron. This is different to the peaking trend of hardness. Figure 3 shows the Cu concentration dependence of conductivity measured for another series of as-quenched

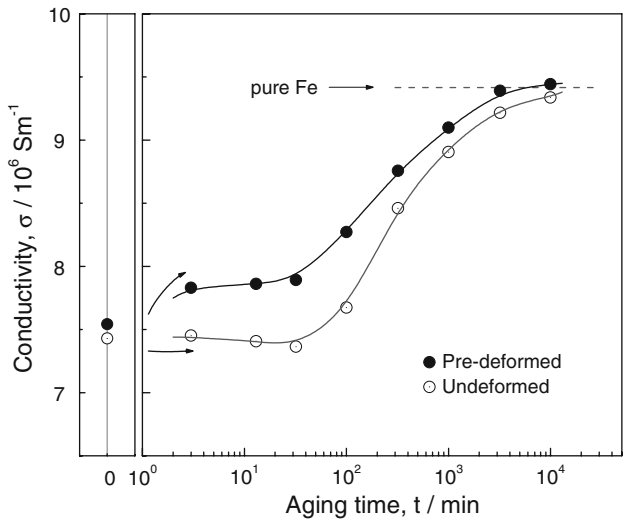

Fig. 2 Aging time dependence of conductivity for pre-deformed and undeformed Fe–Cu alloys

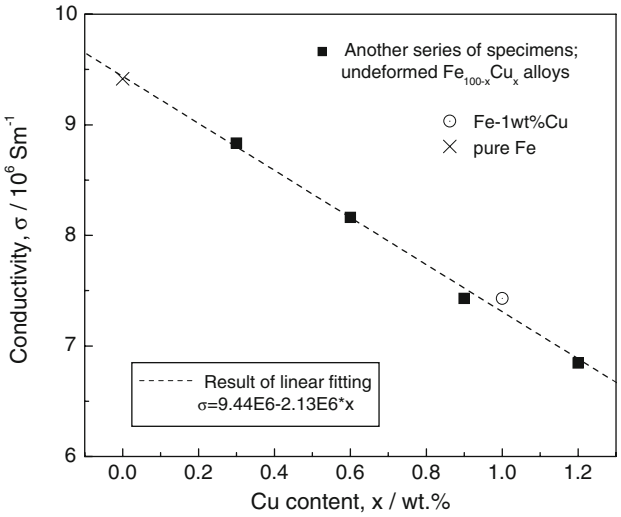

Fig. 3 Cu concentration dependence of conductivity for as-quenched Fe–Cu alloys measured at room temperature

Fe–Cu alloys in solid-solution state. The conductivity almost linearly decreased with increasing Cu content, which suggests conduction electrons are effectively scattered by Cu solute atoms. Although the precipitate contribution to the conductivity also should be considered at the over aged state [14], the increasing trend observed in Fig. 2 is primarily caused by a reduction of Cu solute atoms during the precipitation process. At the initial aging stage, the thermal treatment notably causes an abrupt jump in conductivity in the pre-deformed specimen but not in the undeformed specimen (arrows in Fig. 2). In addition to the initial increase of hardness, this abrupt jump is additional evidence for the enhancement of precipitation by pre-deformation.

Microstructure

Figure 4 shows typical TEM images of pre-deformed and undeformed Fe–Cu alloys at the over-aging state (aged for 2×10^4 min). Both images show many precipitates with diameters measuring tens of nanometers. The crystal structure of these precipitates was determined to be face-centered cubic and the Kurdjumov-Sacks orientational relationship to the matrix was confirmed from the diffraction patterns. The morphology of precipitation is, however, slightly different; in the pre-deformed specimen several dislocations are present and the precipitates are formed within the matrix and at dislocations (Fig. 4a). Regarding the initial aging state, the formation of coherent precipitates, body-centered cubic (bcc) Cu, can be expected [12, 13]. However, clear TEM images of these precipitates could not be obtained probably due to their coherency and small size. During the initial aging stage, it is plausible that bcc-Cu precipitated preferentially along dislocations in the pre-deformed specimen.

Magnetic hysteresis properties

Figure 5 shows *B–H* curves of (a) pre-deformed and (b) undeformed specimens before and after thermal aging for 1 kmin. In pre-deformed specimen, the *B–H* curve of the unaged specimen shows relatively small slope (Fig. 5a), and it is hardly magnetized due to its high dislocation density. Thermal aging caused an increase of the slope (Fig. 5a), whereas a decrease in undeformed specimen (Fig. 5b). The insets of Fig. 5 are magnifications of each *B–H* curve around the coercive force. The coercive force also shows opposite behavior between the two specimens; a decrease in pre-deformed specimen but an increase in the undeformed specimen by thermal aging (insets in Fig. 5). To confirm these trends, aging time dependence of the coercive force is summarized in Fig. 6. Opposite changes clearly occur by thermal aging; a decreasing trend for the pre-deformed specimen and an increasing trend for the undeformed specimen. The inset of Fig. 6 is a magnification of the data for the undeformed specimen. During the over-aging state the change is not large but the coercive force of the undeformed specimen seems to be decreasing which is consistent with previous reports [9, 10].

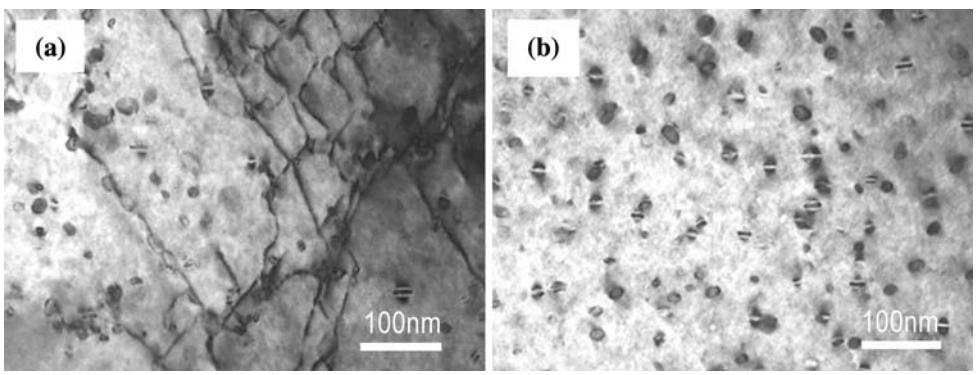

Fig. 4 TEM images after 2×10^4 min aging. **a** Pre-deformed and **b** undeformed Fe–Cu alloys

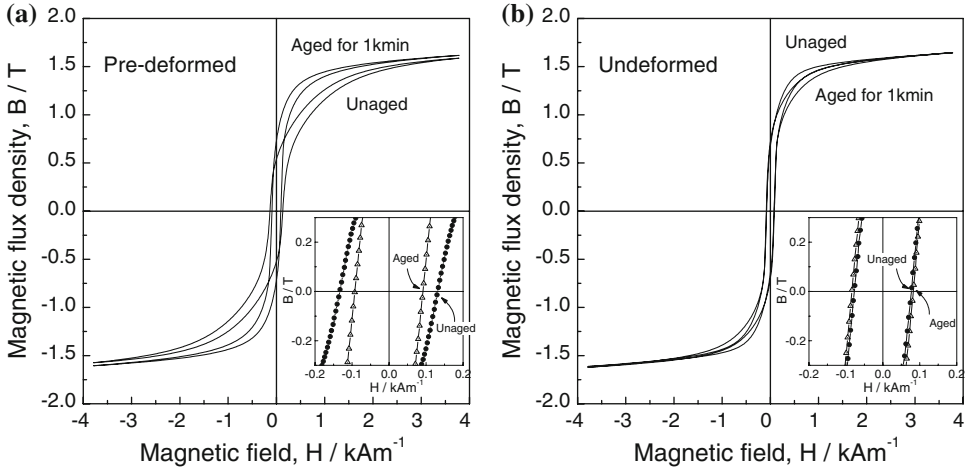

Fig. 5 Magnetic hysteresis loops of unaged and aged Fe–Cu alloys. **a** Pre-deformed and **b** undeformed specimens

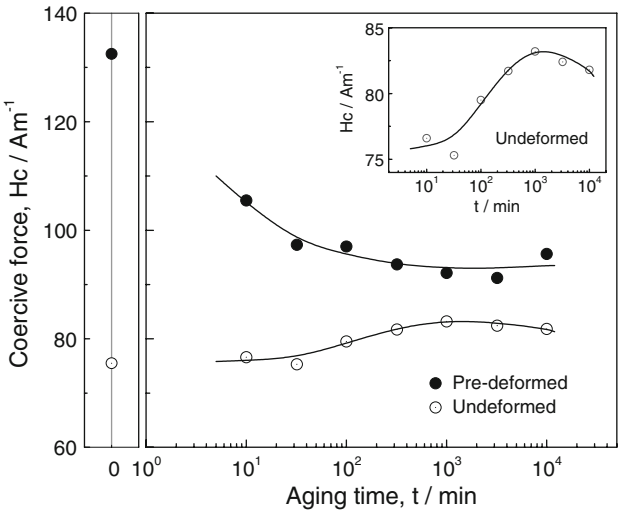

Fig. 6 Aging time dependence of the coercive force of pre-deformed and undeformed Fe–Cu alloys

Discussion

We propose a mechanism for the opposite behavior of coercive force by considering the differences observed in the precipitation process. The coercive force generally reflects the hindrance of magnetic domain wall movement which is caused by the stress field around lattice defects through magneto-elastic interaction [5, 6]. Due to the stress field of dislocations, the coercive force of pre-deformed specimen is much larger than that of undeformed specimen before thermal aging (Fig. 6). The effect of thermal aging on internal stress can be considered as follows. Since the atomic volume of bcc-Cu is larger than that of bcc-Fe [15], formation of coherent Cu precipitates produces an additional stress field around the precipitates. The internal stress of the undeformed specimen would initially increase by thermal aging and turn to decrease due to the structural changes and coarsening of the precipitates. The peaking trend of the coercive force (inset of Fig. 6) is attributed to such a process. The mechanism for the pre-deformed specimen is not as simple due to its high dislocation density and additionally the behavior of internal stress around the dislocation needs to be considered. Two mechanisms are plausible. The first is a compensation of the initial stress field which is a compound effect that originates from the coexistence of dislocations and precipitates. Pre-deformation results in Cu precipitation at dislocations as described before. This probably occurs to reduce the elastic energy of the system. The stress field inherent in precipitates thus compensates for the initial stress field around a dislocation. This compensation reduces the hindrance of magnetic domain wall movement and thus the coercive force decreases. The second mechanism is a modification of the dislocation arrangement. The applied aging temperature of 773 K is relatively low and does not induce re-crystallization in pre-deformed microstructures. However, a small alteration of the dislocation arrangement due to thermal activation of dislocation motion could occur at this low temperature [16]. This modification of dislocation arrangement may affect magnetic properties. While future study is needed to determine the dominant mechanism, the first mechanism cannot be neglected as this study has provided evidence of precipitate formation at dislocations.

It is notable that the coercive force of neutron irradiated RPV steels showed a decreasing trend at high fluence [17]. Neutron irradiation defects, produced by cascade damage, are usually treated as being uniformly distributed in a matrix. However, it has been reported that nano-size defect clusters can accumulate near dislocations because of their mutual elastic interaction [18, 19]. In this case, the stress field of a dislocation that initially exists in RPV steel would be compensated for by the stress field of irradiation defects. This compound effect between dislocations and irradiation defects causes a decrease in the coercive force. This is similar to the situation for the coercive force of

pre-deformed Fe–Cu model alloys as discussed above. The results of this study are quite relevant to understand the magnetic properties of irradiated RPV steels. The correlation between ductile–brittle transition temperature (DBTT) and magnetic parameters of irradiated RPV steels is not simple [17]. The present study helps us to understand the correlation mechanism, which is important to establish a reliable magnetic NDE on irradiation embrittlement.

Conclusions

The precipitation process and magnetic properties of pre-deformed Fe–Cu model alloy were investigated by systematically varying the aging time. Pre-deformation enhanced Cu precipitation and caused formation of precipitates at dislocations. The coercive force of the pre-deformed specimen decreased with increasing aging time suggesting a decrease of the initial stress field of dislocations. This phenomenon could be related to compound effects due to the coexistence of lattice defects and this study provides a key to understand the magnetic properties of irradiated RPV steel.

Acknowledgement This research was partly supported under contract with the Japan Nuclear Energy Safety Organization (JNES) and in part by a Grant-in-Aid for Scientific Research (S), No. 141020345, and (B), No. 20360416, from the Ministry of Education, Culture, Sports, Science and Technology of Japan.

References

1. Odette GR, Lucas GE (1998) Radiat Eff Defects Solids 144:189
2. Fukuya K, Ohno K, Nakata H, Dumbill S, Hyde JM (2003) J Nucl Mater 312:163
3. Nagai Y, Toyama T, Nishiyama Y, Suzuki M, Tang Z, Hasegawa M (2005) Appl Phys Lett 87:261920/1-3
4. Burke MG, Watanabe M, Williams DB, Hyde JM (2006) J Mater Sci 41:4512. doi:10.1007/s10853-006-0084-x
5. Kronmüller H, Fähnle M (2003) Micromagnetism and the microstructure of ferromagnetic solids. Cambridge University Press, UK, p 71
6. Träuble H (1969) In: Berkowitz AE, Kneller E (eds) Magnetism and metallurgy. Academic Press, New York, p 621
7. Park DG, Hong JH, Kim IS, Kim HC (1997) J Mater Sci 32:6141. doi:10.1023/A:1018608321067
8. Pirlog M, Altpeter I, Dobmann G, Hübshen G, Kopp M, Szielasko K (2007) In: Takahashi S, Kikuchi H (eds) Electromagnetic nondestructive evaluation (X). IOS Press, Amsterdam, p 170
9. Takahashi S, Kubota A, Kobayashi S, Kamada Y, Kikuchi H, Ara K (2007) J Mater Process Technol 181:199
10. Vandenbossche L, Konstantinovic MJ, Almazouzi A, Dupre L (2007) J Phys D Appl Phys 40:4114
11. Kamada Y, Park DG, Takahashi S, Kikuchi H, Kobayashi S, Ara K, Hong JH, Park IG (2007) IEEE Trans Magn 43:2701
12. Deschamps A, Militzer M, Poole WJ (2001) ISIJ Int 41:196
13. Zhang C, Enomoto M, Yamashita T, Sano N (2004) Metall Mater Trans A 35A:1253
14. Mathon MH, Barbu A, Dunstetter F, Maury F, Lorenzelli N, de Novion CH (1997) J Nucl Mater 245:224
15. Liu JZ, van de Walle A, Ghosh G and Asta M (2005) Phys Rev B72:144109/1-16
16. Martinez-de-Guerenu A, Arizti F, Diaz-Fuentes M, Gutierrez I (2004) Acta Mater 52:3657
17. Takahashi S, Kikuchi H, Ara K, Ebine N, Kamada Y, Kobayashi S, Suzuki M (2006) J Appl Phys 100:023902/1-6
18. Trinkaus H, Singh BN, Foreman AJE (1997) J Nucl Mater 251:172
19. Ghoniem NM, Singh BN, Sun LZ, Diaz de la Rubela T (2000) J Nucl Mater 276:166